Journal of Integrated
SCIENCE & TECHNOLOGY

Mitigation of Voltage Sag, Swell, PF correction and THD reduction using SST & DC breaker implementation in SST based charging station for EV: Chaotic GWO technique

Dinakar Yeddu#, B. Loveswara Rao*

Department of Electrical and Electronics Engineering, Koneru Lakshmaiah Education Foundation, Vaddeswaram, AP, India.

Received on 15 -Sep-2023, Accepted: 27-Oct-2023 and Published on: 12-Dec-2023

Article

ABSTRACT

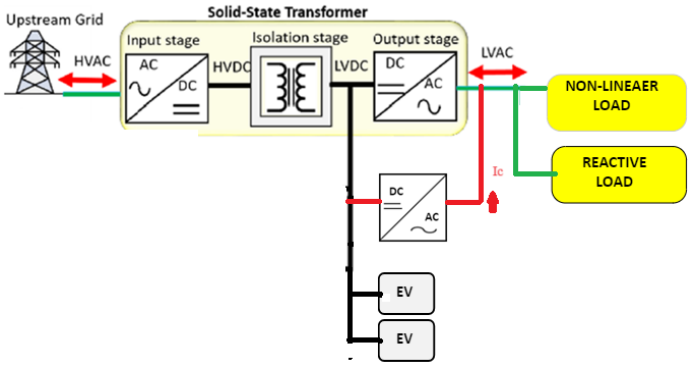

Future electric power distribution will heavily rely on solid-state transformers (SST). Typically, traction and transportation systems use the SST. It can be used for various purposes, though. For instance, the current demand for electric vehicles (EVs) requires the service provider to enhance the infrastructure, such as the number of high-power EV charging stations in urban areas. SST-based charging stations are one design option for high-power charging stations, and they can be linked to the distribution network. The article suggested a novel design for optimizing PI gains using the chaotic GWO algorithm for DC link voltage regulation and a reduction in THD using the SST instead of a shunt active filter in SST-based conductive charging of EVs. Second, the SST is used in place of a series active filter to mitigate voltage sag, swell, and PF correction when faults or abrupt changes in load occur in the AC system. Thirdly, for safety reasons, the SST-based charging of EVs uses a 4P DC breaker. Finally, using the SIMULINK/MATLAB platform, all the cases were simulated, and the results were displayed.

Keywords: solid state transformer(SST),Low frequency transformer(LFT),4P-DC circuit breaker, Chaotic GWO, Battery Pack, Electric vehicle, Charging station, Power converters,Shunt active filter(SAF).

INTRODUCTION

Due to their rapid growth, electric vehicles (EVs) are anticipated to be one of the key contributors to the energy shift in global transportation. The use of transportation is viewed as a desired way to lessen our reliance on fossil fuels and the negative effects they have on the environment, including improved air quality, a reduction in greenhouse gas (GHG) emissions, and climate change. In comparison to conventional internal combustion engine (ICE) vehicles, electric vehicles (EVs) offer zero-emission, extremely reliable, efficient, and low-maintenance automobile.[1]. Due to their promising qualities like free-pollutant gases, no greenhouse gas emissions, and great efficiency, EVs have increasingly gained more attention.[2] An emerging innovation known as the solid state transformer (SST) holds promise for influencing various domains, such as smart grids, traction systems, and renewable energy systems (RESs). Some advantages of SST over traditional low-frequency transformers (LFT) include reactive power correction, voltage control, power distribution management, voltage sag correction, bidirectional power transfer, fault current restriction, harmonic blocking, and electrical isolation. Notably, SST offers the significant benefit of reduced size and weight.[3]

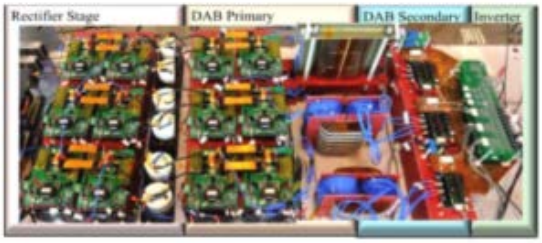

Figure 1. The external appearance of the high-frequency solid-state transformer.

*Corresponding Author: Prof. B. Loveswara Rao
Department of Electrical and Electronics Engineering, Koneru Lakshmaiah Education Foundation, Vaddeswaram, AP, India.
Tel: +91 9866290922, Email: loveswararao@kluniversity.in
#Research Scholar *Professor

Cite as: J. Integr. Sci. Technol., 2024,12(3), 772
URN:NBN:sciencein.jist.2024.v12.772

https://pubs.thesciencein.org/jist

Figure1 shows the physical appearance of SST and in future EV focus on static charging via WPT systems.[4] The developed countries transport sector is investing in EVs.[5]

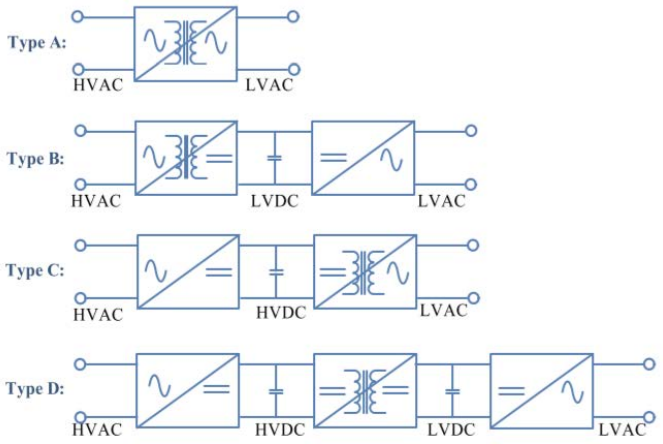

Figure 2 . (a) Single stage, (b)double stage with isolation at the HVDC side, (c) double stage with isolation at the LVAC side, (d)and three stage SST are the four different types of SST architectures.[6]

Figure 2 shows types of SST.When non-linear loads and power electronics equipment are used excessively at the (PCC), harmonic currents are generated, which reduce the quality of the electrical power.[7] The DC-link capacitor, located on the front of the VSI, is used to manage reactive power for the grid.[8] The most commonly used controller in business is the proportional-integral-derivative (PID) controller, but it only performs properly when its settings are correctly tuned.While conventional approaches like Ziegler-Nichols and pole placement have been employed historically for achieving this objective, there has been a growing trend in the adoption of state-of-the-art techniques such as heuristic optimization algorithms in recent times.[9-11]

The heuristic algorithm randomly traverses a huge space until it finds the optimal solution ,or one that is very close to it.The rando m numbers produced by the algorithm are what determine conver gence.[12] Instead of using random numbers, chaotic sequences were used to get better outcomes. This is causing a new heuristics movement that seeks to get better results.[13] The 10 chaotic maps in ref [14] include the Tent, sinusoidal, singer, piecewise, logistic, iterative, sine, Gauss/mouse, circle, and Chebyshev maps. Grey wolf optimization is utilized to fine-tune the PI, and the circle map's chaotic sequence is employed to further enhance its efficiency. Despite the many advantages of the DC grid, its advancement has been constrained by the challenges of stopping fault currents. Most AC breakers are not useful because the DC grid does not have a natural current-zero crossover like the AC grid does.[15]

The current study reports the a novel design of an SST-based DC conduction charging system, and control strategies for THD reduction by using SST. The Ch-GWO, simulation and analysis of mitigation capabilities of SST; and further DC breaker implementation in the protection scenario and their simulation.

DESIGN OF SST BASED CHARGING STATION AND THD REDUCTION BY USING SST

2.1. SST Topology

Solid-state transformer technology has advanced rapidly during the past 20 years. Solid state transformers are already replacing low-frequency transformers in traction applications as a result. This results in considerable weight and volume reductions as well as increased dependability.[16] To charge the EVs, the SST can take the place of the conventional transformer. Figure 3 below shows the solid-state transformer's block diagram.

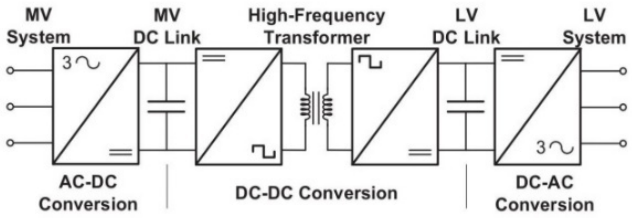

Figure 3. SST three stages block diagram[17]

A feature of the SST architecture makes it possible to power DC loads. It is predicted that the SST configuration's conversion stages will have an overall efficiency of 94%.[18] (AC-DC,DC-DC,DC-AC).

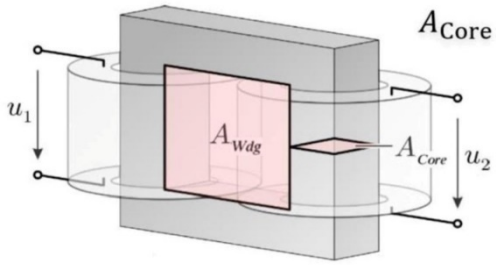

Figure 4. TR core[19]

$$\text{Area Product: Acore. Awdg} = \sqrt{2}/\pi \ \frac{P_t}{K_w J_{rms} B_{max} f}$$

$$\text{Volume: V} \propto \left(A_{core} A_{wdg}\right)^{3/4} \propto \frac{1}{(f)^{3/4}} \qquad (1)$$

The area product demonstrates that a transformer's total core flux density (BMAXT) and winding current density (JRMS) can be maintained while having its volume and weight decreased. Eq. (1) displays the transmitting power. Equation (2) displays the transformer design equation.TR core is shown in Figure 4.

$$V_{pri} = \sqrt{2}\,.\,\pi.\,f.\,N_{pri}.\,\phi_m = 4.44.\,f.\,N_{pri} B_m.\,A \qquad (2)$$

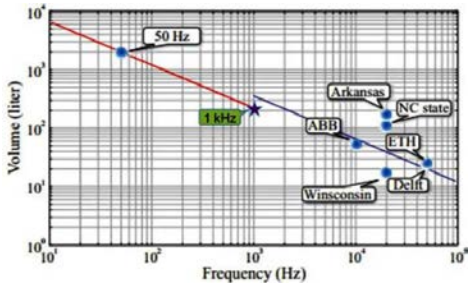

Figure 5. Transformer Volume vs Frequency[20]

Systems with volume and weight restrictions would benefit the most from SSTs' higher power transmission efficiency. With MF transformers, future differentiation is more manageable than with other discrete power electronic converters that connect to MV via a low-voltage (LV) input. Line and load disruptions are controlled using an SST. The blue line in Figure 5 has a silicon steel core, where as the red line has a ferrite core. For frequencies between 1 and 1.5 KHz, silicon core material is appropriate.

2.2 A solid-state transformer with a capacity of 1 MVA, designed for conversion between 11 kV AC input voltage and two output voltages: 415V AC and 800V DC.

In today's power networks, transformers serve the crucial functions of voltage adjustment and electrical isolation. These components are dependable and effective, but their passive design significantly restricts control options. Regional Solid State Transformers (SSTs), which operate as power electronic networks, establish connections between low-voltage AC or DC distribution systems, such as microgrids, and medium-voltage grids. SSTs offer a high level of controllability, stability, and electrical isolation, enabling functionalities like reactive power regulation, active harmonic filtering, and equitable distribution of peak loads. In this context, a fully rated 80 kW converter cell has been successfully developed, considering both the bidirectional capabilities of the distribution-level SST system and its efficiency and power density.

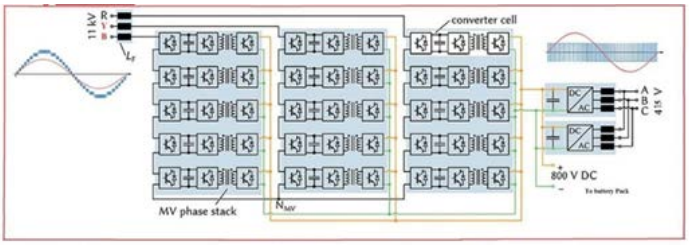

Figure 6. SST schematic diagram[21].

2.3 Scenario-1, when the input is alternating current (AC), the mathematical modeling is as follows.

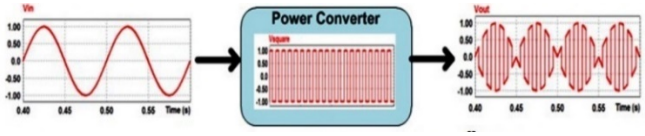

$$V_{in} = \sqrt{2}\, V_{in.rms}.\sin(\omega_s\,.\,t) \;\; * \;\; S_{square} = \frac{4}{\pi}.\sum_{n=1,3,5}^{\infty}\frac{1}{n}\cos(n.\,\omega_{sq}\,.\,t)$$

$$V_{out}=V_{in.rms}\begin{bmatrix} 0.9.\sin(\omega_{sq}\pm\omega_s).\mathrm{t}) \\ +\,0.23.\sin(3\omega_{sq}\pm\omega_s).\mathrm{t}) \\ +0.15.\sin(5\omega_{sq}\pm\omega_s).\mathrm{t}) \\ +\,high\ order\ terms \end{bmatrix} \qquad (3)$$

With the help of the switching function ,we get high-frequency AC from low-frequency AC input. The output voltage's frequency spectrum (FFT), which is depicted in Figure 7 supports the equations.

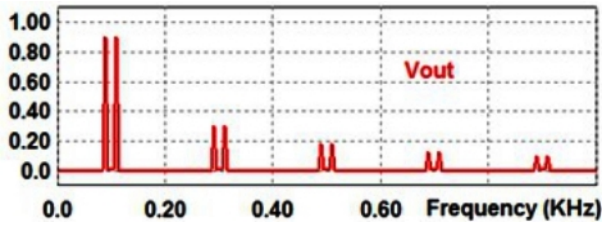

Figure 7. square wave switching function for AC input.

2.4 Scenario-2: When working with solar integration and the input is in the form of direct current (DC), mathematical modeling is employed

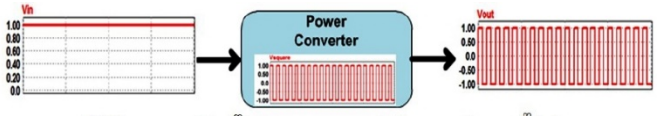

$$V_{in} = V_{dc} \;\; * \;\; S_{square} = \frac{4}{\pi}.\sum_{n=1,3,5}^{\infty}\frac{1}{n}\sin(n.\,\omega_{sq}\,.\,t)$$

$$= \;\; V_{out} = \frac{4}{\pi}.V_{dc}\sum_{n=1,3,5}^{\infty}\frac{1}{n}\sin(n.\,\omega_{sq}\,.\,t) \qquad (4)$$

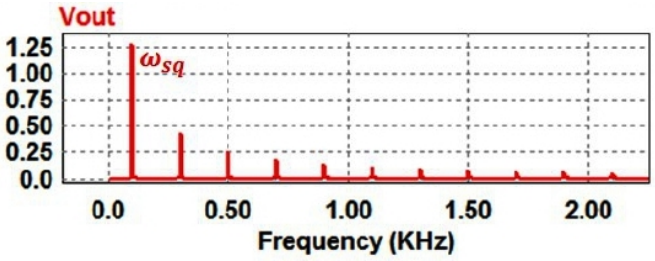

Figure 8. for DC input square wave switching function

A power converter switching function for a situation where a HF square wave is the desired output and a DC signal is the input is depicted in equ-4 The equations are supported by the frequency spectrum of the output voltage (FFT), which is shown in Figure 8.

3. Control strategies -THD reduction by using SST.

3.1 Conventional SAF system.

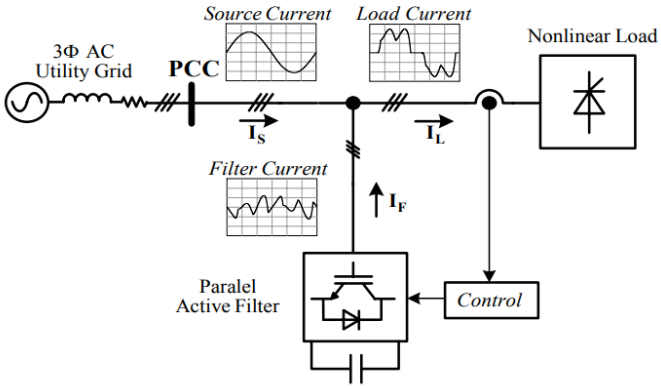

Figure 9. Conventional SAF system [22].

The source current in the preceding diagram Figure 9 must provide both the load current and the compensatory current. The three phase compensating currents I_{ca}, I_{cb}, and I_{cc} are then calculated using the inverse transform from alpha and beta to a, b, and c. It has two blocks: an active filter controller and a PWM block. Power processing is carried out through PWM control, which also creates the compensating current that should be drawn from the system. The real-time instantaneous compensating current references are determined by the active filter controller through signal processing. The PI-controller, which is included in reference current theory, manages harmonic mitigation, and its Kp and Ki gain values must be properly adjusted.

In theory, the voltage across the DC-link capacitor plays a crucial role in regulating harmonic compensation current. The generated harmonic compensation current should ideally match the harmonic current drawn by the nonlinear load, resulting in their cancellation, provided that the voltage across the DC-link capacitor is maintained at the predetermined level.In light of this, the current in the system starts to follow the fundamental frequency's sinusoidal pattern [23].

$$I_S = I_{1L} + I_{dc} \quad (5)$$

3.2 Proposed harmonic filtering in conductive charging system of EV using SST

This system will be connected to an 11 KV high-voltage power distribution network by an active rectifier of the modular type. The high-voltage DC generated by this rectifier enters the DAB (dual active bridge) through its input. Each H-bridge generates a DC voltage, which is sent to DAB, as seen in Fig.6. A dual active bridge or other bidirectional converter (DAB) is present in the stage. It offers isolation. The EV will be charged by the 800V LV-DC bus output.The overall block diagram is shown in Graphical Abstract.

The SST supplies the compensatory current for reactive power compensation in the output, which lowers the THD as shown in Figure 10.

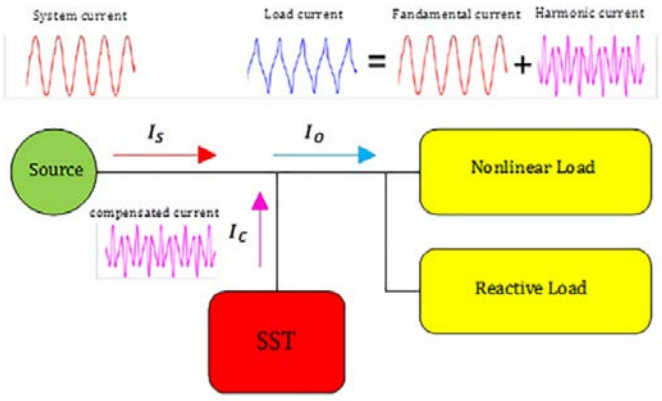

Figure 10. The SST provides reactive power consumption and harmonic filtering[24]

4.0 GREY WOLF OPTIMIZATION(GWO)

Typically referred to as apex predators, grey wolves are at the top of the food chain. They often live in groups of 5 to 12 people and maintain a rigid social hierarchy. They are often divided into three levels: Level one: Alphas; level two: Betas;and level three: Deltas.

Alphas: Here, a male and female are in charge of making decisions on hunting, where to find refuge, when to wake up, and other matters. Alphas sometimes follow the habits of others in the wolf pack and the group as a whole when making decisions. Because the alpha is the dominant one, the other wolves submit to him by holding their tails down. This demonstrates the group's organization and discipline.

Beta: They are the wolves of the subordinates who support the alpha in making decisions or other group tasks. The ideal contender in the event that the alpha wolves pass away or get very old is either a male or a female. Alternatively put, they are Delta: They are the lowest-ranking, which makes them the scapegoat. They are allowed to eat last because everyone else is more powerful. Despite the fact that they don't have any particular significance, they don't get lost in the crowd because they don't cause any issues. They are sometimes referred to as group babysitters at times. This GWO, which is depicted in Figure 11, is a new meta-heuristic technique that relies on swarm intelligence and is inspired by the thought of grey wolves when they are seeking prey.[25] They remain as a pack and are placed in a position to conduct the hunting process. The mathematical approach is designed by giving the group the best fittest answer, which is then followed by the,and groups. Equations 14 and 15 are used to describe how they construct a closed path around the injured in order to start pursuing the prey.

$$\vec{D} = |\vec{c}\vec{x}_P(t) - \vec{x}(t)| \quad (6)$$

$$\vec{x}(t+1) = |\vec{x}_p(t) - \vec{A} \cdot \vec{D}| \quad (7)$$

't' in equation (6) stands for the current iteration. Where A and C are the coefficient vectors provided in equations (6) and (7), X and XP vectors represent the position of the injured Grey wolf and the injured position, respectively.

$$\vec{A} = 2 \cdot \vec{a}.\vec{r_1} - \vec{a} \quad (8)$$

$$\vec{c} = 2 \cdot \vec{r_2} \quad (9)$$

In equations (8)–(9), the components 'a' decrease from 2 to 0 during iteration, while r1 and r2 denote the random vector that changes in the range of [0, 1]. Equations (10–15) provide a mathematical language for evaluating the hunting process.

$$\overrightarrow{D_\alpha} = |\overrightarrow{C_1}.\overrightarrow{X_\alpha} - \overrightarrow{X}| \quad (10)$$

$$\overrightarrow{D_\beta} = |\overrightarrow{C_2}.\overrightarrow{X_\beta} - \overrightarrow{X}| \quad (11)$$

$$\overrightarrow{D_\delta} = |\overrightarrow{C_3}.\overrightarrow{X_\delta} - \overrightarrow{X}| \quad (12)$$

$$\overrightarrow{X_1} = \overrightarrow{X_\alpha} - \overrightarrow{A_1}.(\overrightarrow{D_\alpha}) \quad (13)$$

$$\overrightarrow{X_2} = \overrightarrow{X_\beta} - \overrightarrow{A_2}.(\overrightarrow{D_\beta}) \quad (14)$$

$$\overrightarrow{X_3} = \overrightarrow{X_\delta} . -\overrightarrow{A_3}.(\overrightarrow{D_\delta}) \quad (15)$$

$$\overrightarrow{X}(t+1) = (\overrightarrow{X_1} + \overrightarrow{X_2} + \overrightarrow{X_3})/3 \quad (16)$$

The average value of positions of α, β and δ wolves are found to be the best position of prey which is given in Eq. 16

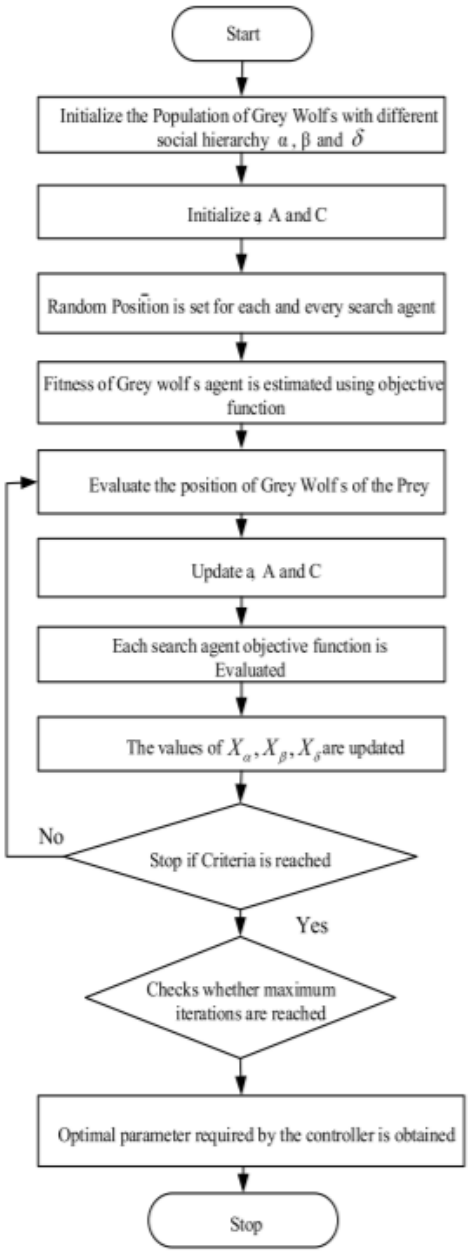

(a)

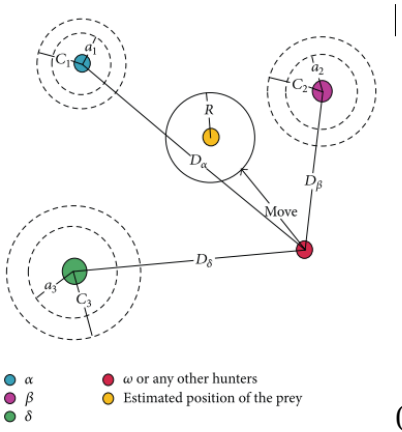

(b)

Figure 11.(a) Flow chart of GWO (b) Position update in GWO[26]

4.1 The novel Chaotic Grey wolf optimization.

Today's metaheuristic algorithms often make use of randomness or particular parameters that need to be changed. Choosing the parameters, though, could be challenging because they might change based on the dataset. So it is possible to successfully resolve the aforementioned problem by using chaos. Chaos is characterized by randomness, non-repetition, ergodicity, and the capacity for the initial condition to alter future behavior's nonlinearity.12 different chaotic maps exist.The circular chaotic map equation, which is described in Eq. (17) is used in the ref [27],

$$x_{k+1} = \mathrm{mod}(x_k + \beta - (\frac{\alpha}{2\pi})\sin(2\pi x_k), 1) \quad (17)$$

$$\alpha = 0.5\,; \beta = 0.2$$

The circle chaotic map visualization is shown in Figure 12.

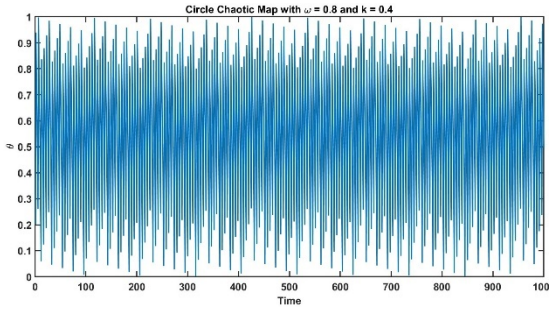

Figure 12. circle chaotic map visualization

The combination of GWO and the chaotic map gives the proposed Ch-GWO . The random value is initiated using the chaotic circle map in code.

```
function r = chaotic_map()
  persistent x;
  if isempty(x)
    x = rand(); % Initialize with a random value between 0 and 1
  end
  mu = 4; % Chaotic parameter (you can adjust this)
  x = mod(mu * x * (1 - x), 1); % Circular map operation
  r = x;
end
```

4.2 PI controller

The Problem Definition and Objective Function

The algorithms' primary goal is to reduce the source current's THD (total harmonic distortion).The Ch-GWO suggested algorithm tunes and optimizes the PI controller gains Kp and Ki to achieve this and the block diagram is shown in Figure 13

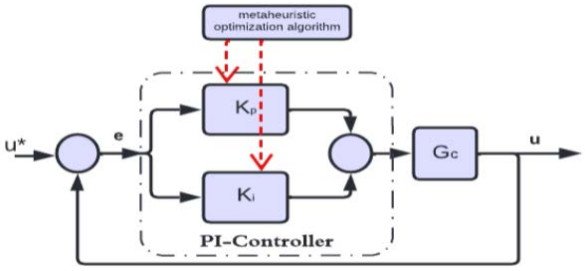

Figure 13. optimization Algorithms controlled PI

Eqns 19 & 20 gives Transfer function & output u(t) of the PI controller.

$$THD_i = \sqrt{\frac{\sum_{k=2}^{kmax} I_k^2}{I_1^2}} \quad (18)$$

$$\boldsymbol{G_C}(S)=\boldsymbol{K_p} + \boldsymbol{k_i}/S \quad (19)$$

$$u(t)=e(t) + k_i \int_0^1 e(t)\ .dt \quad (20)$$

where e(t) is the error Vdc and the (Vdc_{ref}).

The capacitor voltage ought to be constant if there is no actual power transfer between the filter and the AC grid. The VSI practically uses a small amount of real power for its switching action, as was already explained. The magnitudes of (isa, isb, isc) are approximately equivalent to the magnitudes of i_a, i_b, and i_c when the VSI switches are operated at a high frequency. As a result, it is presumptive that the closed-loop transfer function is one [28]and is depicted in Figure 14

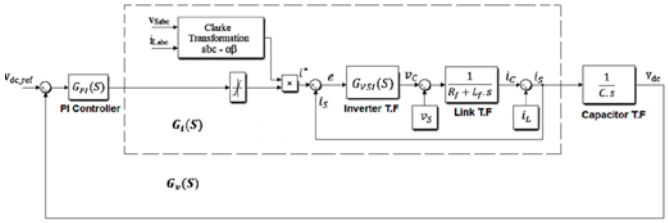

Figure 14. cascade control loops of current and voltage.

$$\frac{v_{dc}}{v_{dc\_ref}} = \frac{\frac{K_p \cdot K_i}{C}}{s^2 + \frac{K_p}{C} \cdot s + \frac{K_p \cdot K_i}{C}} \quad (21)$$

Table 1. SST Parameters

Parameters	Values
V_i	11KV-AC
V_o	DC-800V
Cap_{MV}	500nF
Cap_{LV}	70 μF
TR mag ind (L_h)	4.1mH
TR lea ind ($L\sigma$)	195μH
Fsw	50khz

Table 2 . Parameters of DC/AC converter of SST

Parameters	Values
V_S	380Vph-ph
Freq	50Hz
Source impedance	Rs=0.1Ω,Ls=10mh
Filter impedance	Ls=1mh
DC-link capacitor	1000microF,400V
Balanced load	10Ω &40mh
Unbalanced load	5Ω,10Ω,30Ω
Dc reference voltage	650V
Kp,Ki	1.2, 20

RESULTS AND ANALYSIS

5.1 Scenario1: Simulation of SST based charging station

The novel SST based charging system, 11KV/1MVA/800V was simulated.[29] The output is 800V DC and waveform is shown in Figure 15 and the parameters are shown in table1

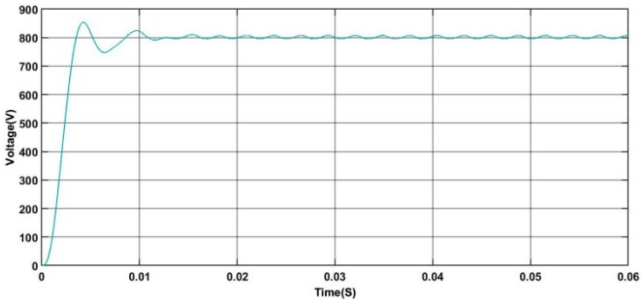

Figure 15. SST output voltage waveform.

5.2 Scenario 2: SST-Filtering the harmonics.

By injecting current and lowering the harmonic current in this situation, the SST is enhancing the power quality. SST functions here as a shunt active filter.Table2 shows the parameters.

5.2.1 Balanced system non-linear load without compensation

In this case only voltage is supplied from SST no control action. Figure 16 shows the load and source currents waveforms , and source current FFT harmonic spectrum shown in the Figure 17, then the THD is 9.05%

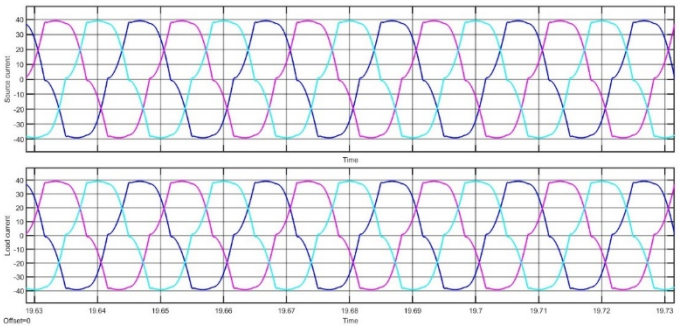

Figure 16. source current & load current before compensation

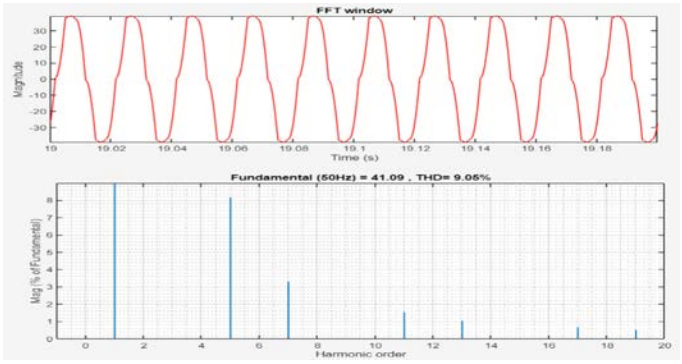

Figure 17. source current FFT analysis

5.2.2 After compensation- with SST connected balanced non-linear load.

After compensation figure 18 shows waveforms of source ,compensating and load currents respectively and THD of source current is 1.32% and its FFT spectrum is shown in figure 19.

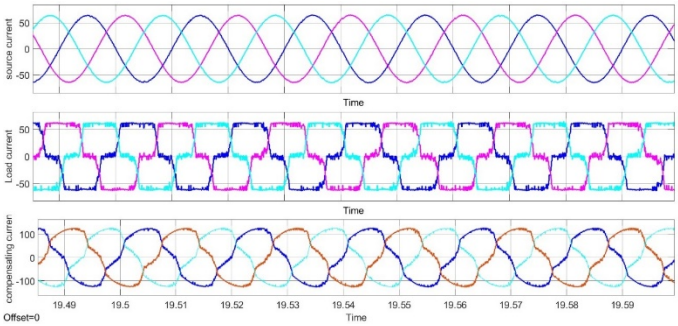

Figure 18. After compensation (a) Source current (b) Compensating current (c) Load current.

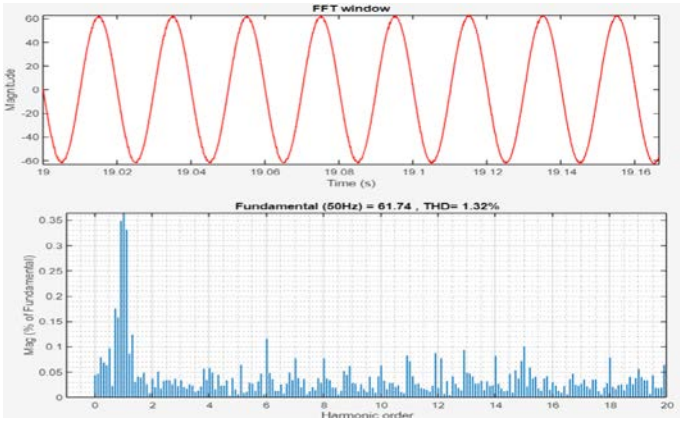

Figure 19 . FFT analysis of source current.

5.2.3 .Unbalanced system non-linear load with out SST filtering action.

In this, SST with an unbalanced 3 phase RL load connected to diode rectifier. The figure 20 shows waveforms of source and load currents respectively. Figure 21 shows the THD spectrum of source current and is 5.47%.

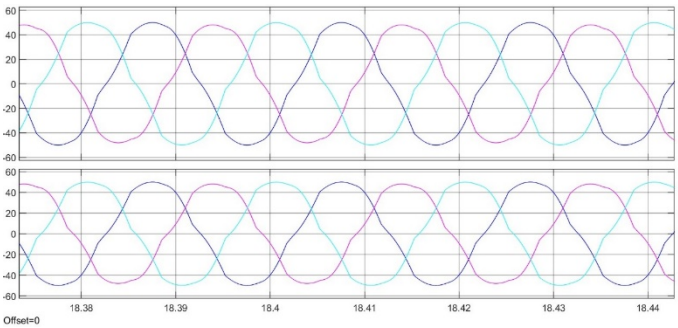

Figure 20. Before compensation unbalanced system (a) source current (b) load current.

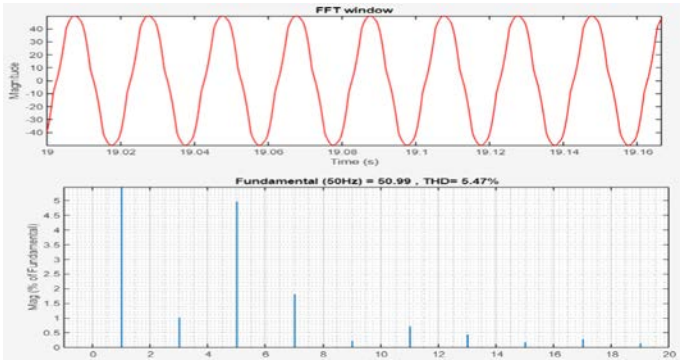

Figure 21.Before compensation unbalanced system fft analysis of source current.

5.2.4 After compensation unbalanced system

The figure 22 shows waveforms of source ,compensating and load currents respectively. Figure 23 shows the FFT spectrum of source current and is 1.96%.

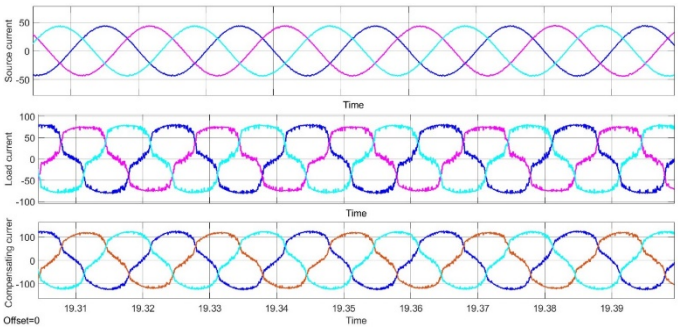

Figure 22. After compensation unbalanced system (a) source current (b) load current.

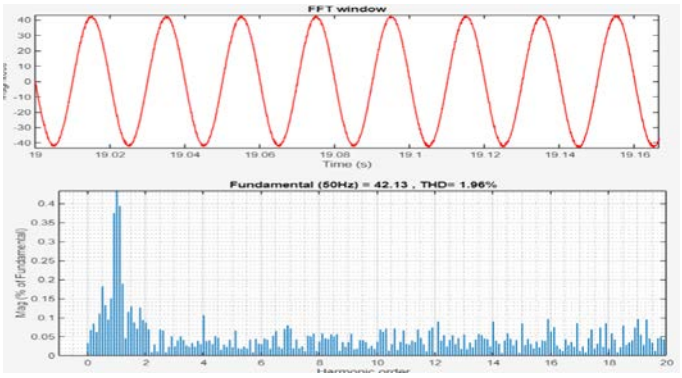

Figure 23. FFT analysis of source current.

5.2.5 After compensation- Balanced system using GWO in SST based filtering

The GWO is a optimization algorithm to minimize the THD of the balanced system .It tunes the Kp and Ki parameters .The values are Kp=88.5357 and kd=0.0001.After compensation source and load currents waveforms and THD of source current spectrum is 1.08%. as shown in figure 24 & figure 25 respectively.

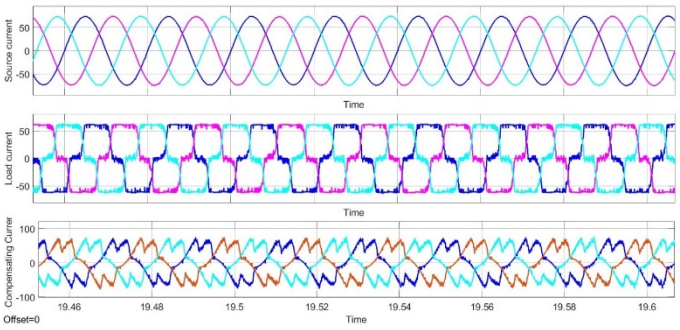

Figure 24. After compensation (a) source current (b) load current.

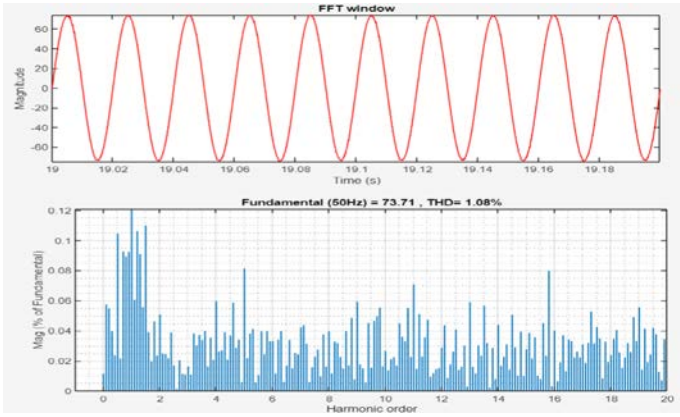

Figure 25. FFT analysis of source current

5.2.6 After compensation -Unbalanced system using GWO in SST filtering

The unbalanced system using the chaotic grey wolf optimization The values are Kp=88.5357 and kd=0.0001.After compensation source and load currents and THD of the source current is 0.98% as shown in figure 26 & figure 27.

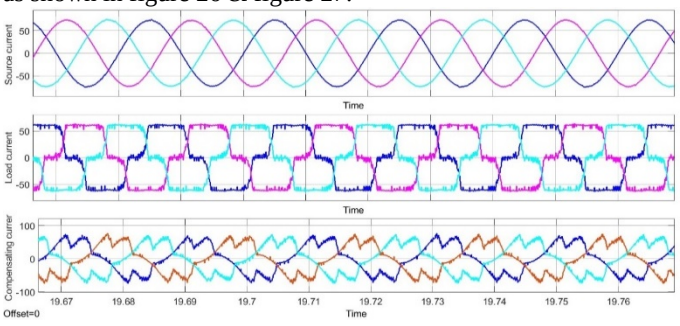

Figure 26.(a)Source current (b) Load current

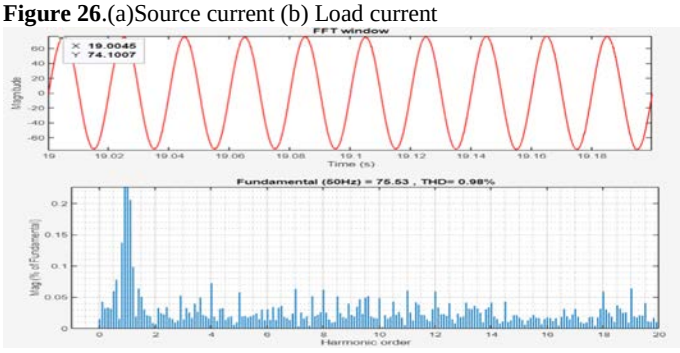

Figure 27. FFT analysis of source current

5.2.7. Balanced system After compensation using chaotic GWO in SST based filtering

In a balanced system using chaotic GWO pi gains are tuned the Kp=99.9804 and ki =0.078521values.After compensation the source and load current waveforms and the THD of the source current is 1.03% as shown in figure 28 and figure 29 respectively.

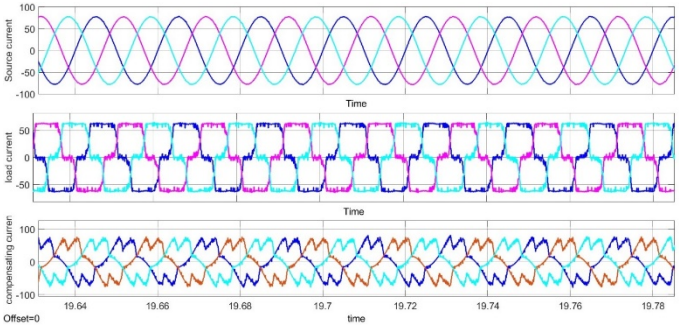

Figure 28.After compensation (a) source current (b) load current.

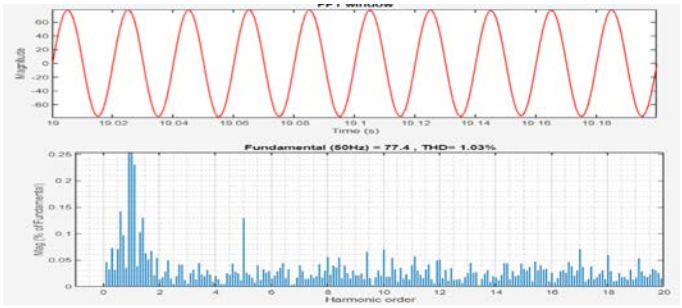

Figure 29 FFT analysis of source current

5.2.8 after compensation -Un Balanced system using chaotic-GWO with SST filtering

In the unbalanced system after compensation using ch-GWO to tune pi values .The Kp=99.9804 and K_i=0.078521.The source and load current waveforms and THD is 0.94% as shown in figure 30 and figure.31 respectively.

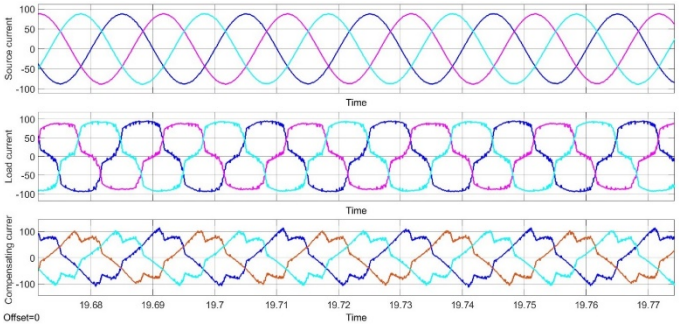

Figure 30 After compensation (a) source current (b) compensating current (c) Load current.

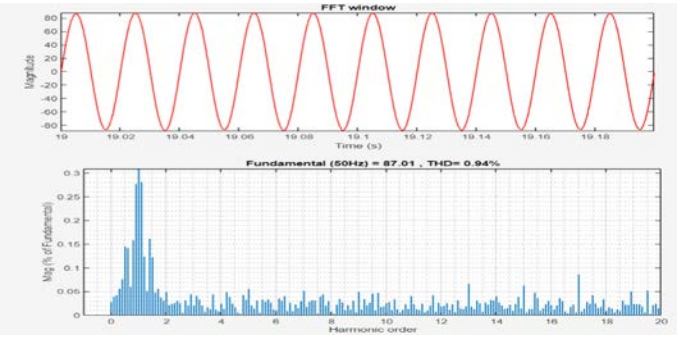

Figure 31. FFT analysis of source current.

5.3 THDs of source current

Table 3 shows the THD of above, all the scenarios

Table.3: THD'S of different scenarios.

No	Load description	%source current THD
1	Balanced system non-linear load without SST	9.05
2	Balanced system non-linear load with SST	1.32
3	Unbalanced system non-linear load without SST	5.47
4	Unbalanced system non-linear load with SST	1.96
5	Balanced system non-linear load with SST tuned by GWO	1.08
6	Unbalanced system non -linear load with SST tuned by GWO	0.85
7	Balanced system non-linear load with SST tuned by Ch-GWO	1.03
8	Un Balanced system non-linear load with SST tuned by Ch-GWO	0.94

5.4. With connected SST and PI tuned by ch-GWO

Table 4 shows the %THD comparision of proposed and existing algorithms

Table .4 .% THD comparison

Method	% THD			
	Before compensation		After compensation	
	Balance system	Unbalance	Balance system	Unbalance
Proposed PI	9.05	5.47	1.32	1.96
Proposed GWO	--	---	1.08	0.85
Proposed Ch-GWO	--	---	1.03	0.94
PSO[18]	11.4427	11.90	2.11	3.42
ACO PI[19]	28.01	-	3.72	-
GA[20]	31.66	-	4.56	-

IMPLEMENTATION OF PROTECTION SYSTEM IN SST BASED CHARGING STATION

6.1 SST Mitigation capabilities under fault conditions-protection scenario.

The proposed SST removes voltage sag and swells and corrects the input PF. Ref [30] and table 5 shows the parameters of SST.

Table 5. Parameters of SST

Parameters	Values
V_i	11KV-AC
V_o	DC-800V
Cap_{MV}	500nF
Cap_{LV}	70 μF
TR mag ind (L_h)	4.1mH
TR lea ind ($L\sigma$)	195μH
Fsw	50khz
Output line voltage	380V

6.2 PF correction

The figure .32 shows the waveforms of input voltage and current .SST -controller makes the q component to zero of input current for lag load.

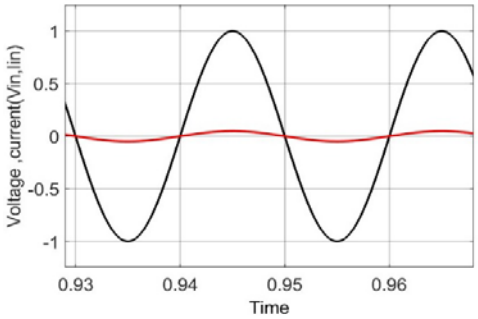

Figure 32. SST current and voltage waveforms in inductive load (a). single phase input voltage and current.

6.3 Response to SAG voltage

Figure 33 (a) shows three phase balanced voltage sag with 30% depth created at 0.4-0.5s at input voltage. Figure.33(b), the load voltage is maintained constant with the compensating voltage shown in Figure 33(c) by using the SST.

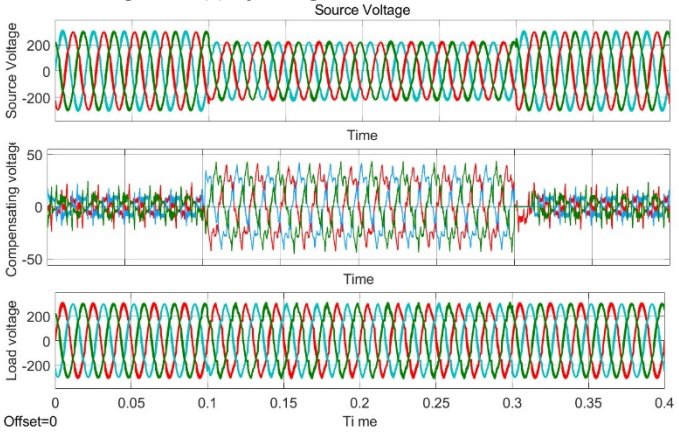

Figure 33 (a) Input line voltage (b) compensating voltage (c) output voltage.

6.4 Responses to swell voltage

The three-phase balanced voltage swell at input voltage is depicted in Figure 34(a). Between t = 0.4 and t = 0.5 s is the swell period. The load voltage in figure 34(b) is maintained constant with the compensating voltage in figure 34(c) by using the SST.

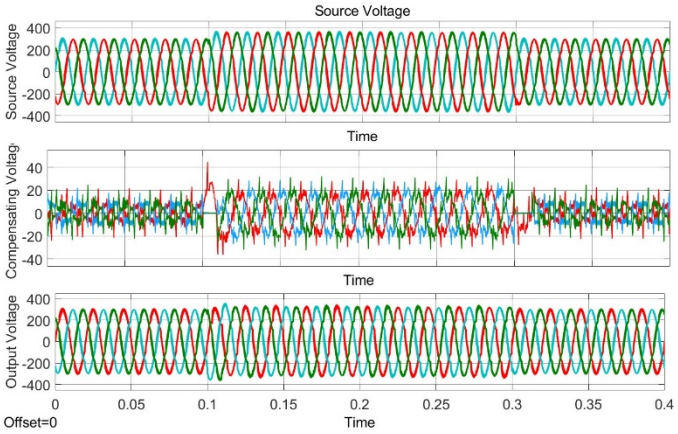

Figure 34 (a) Input line voltage (b) Compensating voltage (c) Output voltage

IMPLEMENTATION OF 4P DC BREAKER IN PROTECTION SYSTEM OF CHARGING STATION.

DC system-Interrupting direct current.

Direct current provides distinct challenges than alternating current because it is more difficult to extinguish an arc switching current. At each half cycle, there is a natural flow of current through zero as shown in figure 35(a) which corresponds to the quenching of the arc during circuit opening. Since there is no such natural passage for direct current, as shown in figure 35(b) arc extinction must be ensured by forcing the current to flow through zero (null).[31]

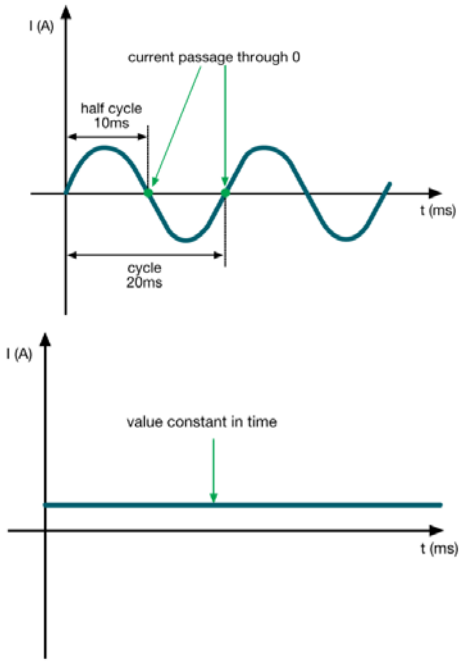

Figure 35. (a)Alternating current.(b)Direct current.

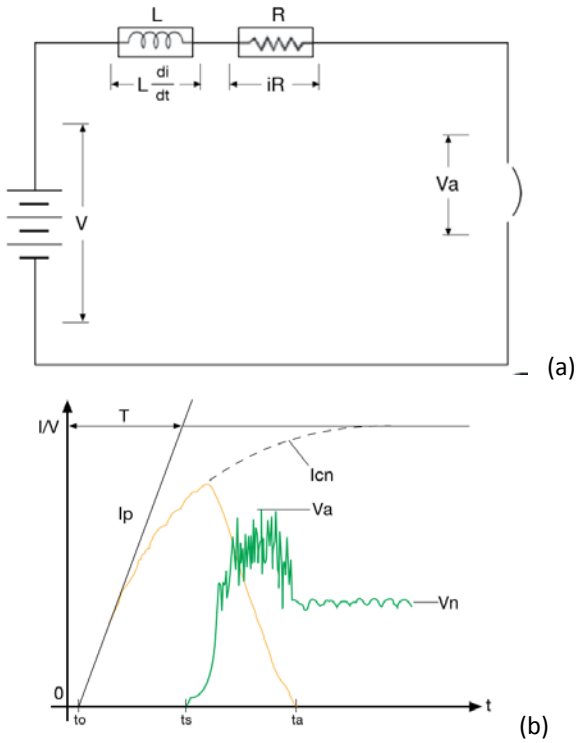

Figure 36 (a) circuit diagram (b) graphical representation

$$V=Ldi/dt+Ri+Va \quad (22)$$

The formula can be written as

$$Ldi/dt=V-Ri-Va \quad (23)$$

For the arc to extinguish $di/dt<0$

Figure 36(a) depicts DC circuit diagram.According to the circuit's time constant, the current begins to increase As per figure 36(b) when a short circuit occurs at the instant ‘ to’. An arc starts at the instant ‘ts’ when the circuit breaker contacts start to separate.

When using a 4P DC breaker, which is utilized in SST-based conductive charging systems, two poles are made in series with one another so that the arc's resistance rises and the arc can be quenched more quickly than with a 2-Pole arrangement and is depicted in figure 37.

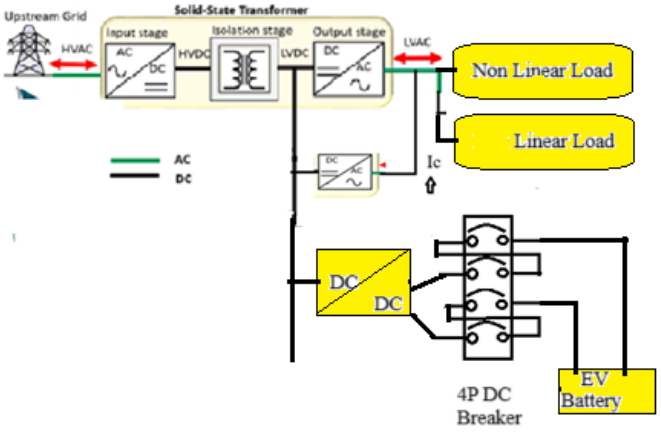

Figure 37. Implementation of 4P dc breaker in SST-EV charging station.

Matlab model for DC protection of Battery pack.

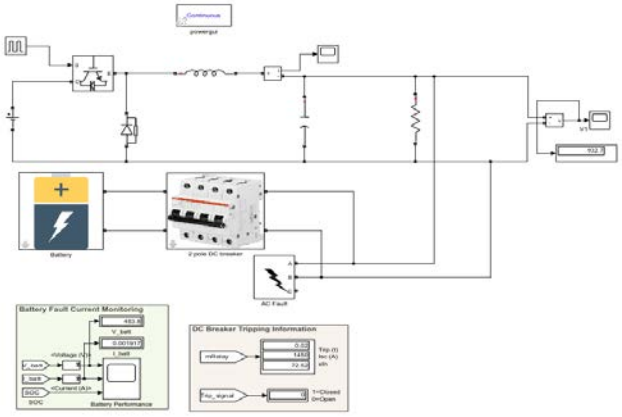

Figure 38. Matlab model for DC protection of Battery pack.

In the above figure 38 for dc protection of battery pack is modelled in simulink.The above model is simulated and the LG fault is applied at 0.1s and the Tsim=0.5s.The 4P dc breaker (2p in series for +ve pole and 2p in series for -Ve pole).detected the fault and clear the fault in in 0.02s.Table6 shows the battery spec and MCB details.

Table 6. Battery specifications & MCB details

Parameter	Values
Nominal voltage	450V
Rated capacity (AH)	33.33
Initial SOC	50
4P MCB-Rated current	20A
SC level	1.5KA

Waveforms of the simulation

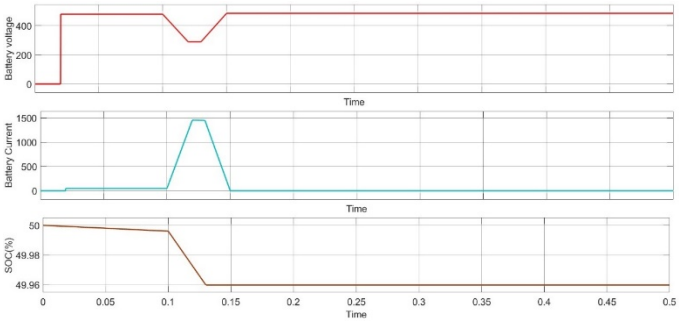

Figure 39. (a) Battery voltage (b)Battery current (c) SOC(%)

As per figure 39, the 4P MCB cleared the fault within 0.02s when a LL fault is created in Simulink.The probability of quenching the arc is higher in a 4P Dc breaker than in a 2P because when two poles are added in series, it increases the resistance of the contacts.

CONCLUSION

The SST will replace the LFT in future. Initially, SST based 11kv/800vdc is simulated and waveforms are presented. Then SST is used as a shunt active filter role there by reducing the total harmonic distortion (THD), and the results are presented. The THD results are compared with out controller & with controller. Then with GWO & chaotic GWO tuned the PI controllers for better performance i.e. THD, according to IEEE 519 and finally compared them with other optimization techniques. The topology described in this paper has many advantages, such as power factor correction, voltage regulation, voltage sag and swell elimination all of them results shown. Finally, we implemented 4p DC breaker for arc extinction in the charging station area which cleared the fault in 0.02s when a LL faults is created, further supported by simulation in MATLAB/SIMULINK platform.

CONFLICTS OF INTEREST

Authors declare no conflict of interest is there for publication of this work

REFERENCES

1. S.S.G. Acharige, M.E. Haque, M.T. Arif, et al. Review of Electric Vehicle Charging Technologies, Standards, Architectures, and Converter Configurations. *IEEE Access* **2023**, 11, 41218-41255.
2. S. Mohammed, J. Jung. A Comprehensive state of the art review of wired /wireless charging technologies for battery electric vehicles Classification/common topologies /future research issues. *IEEE access* **2021**, 27 (9), 19572–85.
3. S.M. Malik, Y. Sun, J. Hu. A novel solid state transformer based control topology for interconnected MV and LV hybrid microgrids. *Energy Reports* **2022**, 8, 10385–10394.
4. D. Yeddu, B.L. Rao. Application of Solid State Transformer in Wireless charging system of EV and voltage profile enhancement by using AI techniques. *J. Integr. Sci. Technol.* **2024**, 12 (1), 705.
5. D. Yeddu, B.L. Rao. A Hybrid Chaotic MPA-PID Controller for Voltage Profile Enhancement in Solid State Transformer-Connected Pantograph System for Charging an Electric Bus. *Int. J. Renew. Energy Res.* **2023**, 13 (2), 899–910.
6. A.L. Eshkevari, A. Mosallanejad, M. Sepasian. In-depth study of the application of solid-state transformer in design of high-power electric vehicle charging stations. *IET Electr. Syst. Transp.* **2020**, 10 (3), 310–319.
7. B. Jahnavi, S.B. Karanki, P.K. Kar. Power quality improvement with D-STATCOM using combined PR and Comb filter-Controller. In *ICPEE 2021 - 2021 1st International Conference on Power Electronics and Energy*; IEEE, **2021**; pp 1–6.
8. N. Pachaivannan, R. Subburam, U. Ramkumar, M. Padmanaban. Fuzzy tuned real and reactive power regulation in GC-VSI for PV systems. *Int. J. Electron.* **2023**, 110 (3), 547–563.
9. S. Ekinci, B. Hekimoğlu, S. Kaya. Tuning of PID Controller for AVR System Using Salp Swarm Algorithm. In *2018 International Conference on Artificial Intelligence and Data Processing, IDAP 2018*; Malatya, Turkey, **2019**; pp 424–429.
10. S. Duman, N. Yörükeren, I.H. Altaş. Gravitational search algorithm for determining controller parameters in an automatic voltage regulator system. *Turkish J. Electr. Eng. Comput. Sci.* **2016**, 24 (4), 2387–2400.
11. M.J. Blondin, J. Sanchis, P. Sicard, J.M. Herrero. New optimal controller tuning method for an AVR system using a simplified Ant Colony Optimization with a new constrained Nelder–Mead algorithm. *Applied Soft Computing Journal*. 2018, pp 216–229.
12. R. Caponetto, L. Fortuna, S. Fazzino, M.G. Xibilia. Chaotic sequences to improve the performance of evolutionary algorithms. *IEEE Transactions on Evolutionary Computation*. 2003, pp 289–304.
13. N.S. Jaddi, S. Abdullah. Optimization of neural network using kidney-inspired algorithm with control of filtration rate and chaotic map for real-world rainfall forecasting. *Eng. Appl. Artif. Intell.* **2018**, 67, 246–259.
14. G.I. Sayed, G. Khoriba, M.H. Haggag. A novel chaotic salp swarm algorithm for global optimization and feature selection. *Appl. Intell.* **2018**, 48 (10), 3462–3481.

15. Y. Gao, Z. He, C. Wang, et al. A new hybrid circuit breaker for DC-application. In *Dianwang Jishu/Power System Technology*; IEEE, **2016**; Vol. 40, pp 1320–1325.
16. M.A. Hannan, P.J. Ker, M.S.H. Lipu, et al. State of the art of solid-state transformers: Advanced topologies, implementation issues, recent progress and improvements. *IEEE Access* **2020**, 8, 19113–19132.
17. D. Atkar, P. Chaturvedi, H.M. Suryawanshi, et al. Solid State Transformer for Electric Vehicle Charging Infrastructure. In *2020 IEEE International Conference on Power Electronics, Smart Grid and Renewable Energy, PESGRE 2020*; **2020**; Vol. PESGRE2020, pp 1–6,.
18. J. Burkard, J. Biela. Hybrid transformers for power quality enhancements in distribution grids - Comparison to alternative concepts. In *NEIS 2018 - Conference on Sustainable Energy Supply and Energy Storage Systems*; **2020**; pp 112–117.
19. P.R. Choube, V.K. Aharwal. Evaluation of Z-Source Inverter Topologies for Power Conditioning Unit for DC Power Supply Systems. *J. Integr. Sci. Technol.* **2022**, 10 (3), 209–214.
20. G. Ortiz, J. Biela, J.W. Kolar. Optimized design of medium frequency transformers with high isolation requirements. In *IECON Proceedings (Industrial Electronics Conference)*; **2010**; pp 631–638.
21. J.E. Huber, J.W. Kolar. Applicability of Solid-State Transformers in Today's and Future Distribution Grids. *IEEE Trans. Smart Grid* **2019**, 10 (1), 317–326.
22. H. Ozkaya, O.S. Senturk, A.M. Hava. Performance enhancement and comparison of discrete time current regulators for parallel active filters. In *2007 European Conference on Power Electronics and Applications*; IEEE, **2007**; pp 1–10.
23. A.A. Eid, A.M.A. Soliman, M.A. Mehanna. Optimize Gain Values of PI-Controller for Active Power Filter Using Mayfly Algorithm. *Int. J. Renew. Energy Res.* **2022**, 12 (4), 1727–1735.
24. H. Shadfar, M. Ghorbani Pashakolaei, A. Akbari Foroud. Solid-state transformers: An overview of the concept, topology, and its applications in the smart grid. *Int. Trans. Electr. Energy Syst.* **2021**, 31 (9), 129961727–1735.
25. A.K. Mishra, S.R. Das, P.K. Ray, et al. PSO-GWO Optimized Fractional Order PID Based Hybrid Shunt Active Power Filter for Power Quality Improvements. *IEEE Access* **2020**, 8, 74497–74512.
26. M.O. Okwu, L.K. Tartibu. Grey Wolf Optimizer. In *Studies in Computational Intelligence*; **2021**; Vol. 927, pp 43–52.
27. J. Too, A.R. Abdullah. Chaotic Atom Search Optimization for Feature Selection. *Arab. J. Sci. Eng.* **2020**, 45 (8), 6063–6079.
28. A.A. Imam, R. Sreerama Kumar, Y.A. Al-Turki. Modeling and simulation of a pi controlled shunt active power filter for power quality enhancement based on p-q theory. *Electron.* **2020**, 9 (4), 637.
29. A. Pidlisecky, R. Knight. FW2_5D: A MATLAB 2.5-D electrical resistivity modeling code. *Comput. Geosci.* **2008**, 34 (12), 1645–1654.
30. M.R. Banaei, E. Salary. Mitigation of voltage sag, swell and power factor correction using solid-state transformer based matrix converter in output stage. *Alexandria Eng. J.* **2014**, 53 (3), 563–572.
31. M.R. Kaisar Rachi, I. Husain. Design and development of a hybrid DC circuit breaker for 380V DC distribution system. In *Conference Proceedings - IEEE Applied Power Electronics Conference and Exposition - APEC*; IEEE, **2021**; pp 1122–1127.